PHYSICAL REVIEW C **96**, 034303 (2017)

Knockout and fragmentation reactions using a broad range of tin isotopes

J. L. Rodríguez-Sánchez,[1,*] J. Benlliure,[1] C. A. Bertulani,[2] J. Vargas,[1,†] Y. Ayyad,[1,‡] H. Alvarez-Pol,[1] J. Atkinson,[3] T. Aumann,[3,4] S. Beceiro-Novo,[1,§] K. Boretzky,[3] M. Caamaño,[1] E. Casarejos,[5] D. Cortina-Gil,[1] J. Díaz-Cortes,[1] P. Díaz Fernández,[1,‖] A. Estrade,[3,6,¶] H. Geissel,[3] A. Kelić-Heil,[3] Yu. A. Litvinov,[3] M. Mostazo,[1] C. Paradela,[1,#] D. Pérez-Loureiro,[1,**] S. Pietri,[3] A. Prochazka,[3] M. Takechi,[3,††] H. Weick,[3] and J. S. Winfield[3]

[1]*Universidad de Santiago de Compostela, E-15782 Santiago de Compostela, Spain*
[2]*Department of Physics and Astronomy, Texas A&M University–Commerce, Commerce, Texas 75429, USA*
[3]*GSI-Helmholtzzentrum für Schwerionenforschung GmbH, D-64291 Darmstadt, Germany*
[4]*Institut für Kernphysik, Technische Universityät Darmstadt, D-64289 Darmstadt, Germany*
[5]*Universidad de Vigo, E-36200 Vigo, Spain*
[6]*Saint Mary's University, Halifax, Nova Scotia B3H 3C3, Canada*

(Received 28 November 2016; revised manuscript received 15 June 2017; published 5 September 2017)

Production cross sections of residual nuclei obtained by knockout and fragmentation reactions of different tin isotopes accelerated at 1*A* GeV have been measured with the fragment separator (FRS) at GSI, Darmstadt. The new measurements are used to investigate the neutron-excess dependence of the neutron- and proton-knockout cross sections. These cross sections are compared to Glauber model calculations coupled to a nuclear de-excitation code in order to investigate the role of the remnant excitations. This bench marking shows an overestimation of the cross sections for the removal of deeply bound nucleons. A phenomenological increase in the excitation energy induced in the remnants produced in these cases allows us to reproduce the measured cross sections.

DOI: 10.1103/PhysRevC.96.034303

I. INTRODUCTION

Peripheral heavy-ion collisions involving few projectile and target nucleons, such as quasifree $(e,e'p)$ and $(p,2p)$ scattering reactions [1–6] or transfer reactions [7], have been widely used to investigate the single-particle structure of the nuclear many-body system. The emergence of fast radioactive beams from the fragmentation of heavy ions was of major importance to the field and offered the possibility of using some of these reactions systematically as a tool for studying unstable nuclei up to the drip lines [8,9].

Reaction studies using radioactive beams are performed in inverse kinematics [10]. This technique, together with the use of knockout reactions, has been shown to be a particularly powerful tool to investigate unstable nuclei, the main observables being the cross sections and the longitudinal momentum distributions of the reaction residues [11–17].

In particular, one-nucleon-knockout cross sections [18] have been used to investigate spectroscopic factors in the framework of the eikonal approximation [14,19]. These studies have shown that the predicted cross sections are systematically too high for deeply bound nucleons, by a factor larger than 3 or 4, while for weakly bound nucleons the model calculations could provide values closer to the measured ones. However, this tendency is not supported by the results obtained in experiments using transfer reactions, where only a weak dependence on the binding energy was observed [20,21]. This discrepancy has been investigated in different works, suggesting that nuclear excitations would reduce the survival probability of the remnants reducing the one-nucleon-knockout cross sections [22–25].

In this context, one-nucleon-knockout cross sections of unstable and stable nuclei from beryllium to uranium have been studied recently in the framework of the abrasion model [26], where the excitation energy gained by the knockout remnant is calculated according to the single particle-hole picture [27]. Then, the de-excitation of the knockout remnant via emission of light particles, such as protons and neutrons, is described according to Weisskopf's formalism [28]. A comparison of this model calculation with a large range of experimental knockout cross sections has suggested a mass-number dependence of the average excitation energy gained by the knockout remnants [26].

To go further, in the present work we provide new data covering a large range in neutron excess to investigate knockout reactions and, in particular, some of the reaction models used for their description. We take advantage of several beams of stable and unstable tin isotopes, at kinetic energies of around 1*A* GeV, to systematically investigate the neutron- and

*Present address: IRFU, CEA, Université Paris-Saclay, F-91191 Gif-sur-Yvette, France.
†Present address: Universidad Santo Tomás, Boyacá, Colombia.
‡Present address: National Superconducting Cyclotron Laboratory, Michigan State University, East Lansing, MI 48824-1321, USA.
§Present address: Department of Physics and Astronomy, Michigan State University, East Lansing, MI 48824-1321, USA.
‖Present address: Institutionen för Fysik, Chalmers Tekniska Högskola, 41296 Göteborg, Sweden.
¶Present address: Department of Physics, Central Michigan University, Mount Pleasant, MI 48858, USA.
#Present address: EC-JRC, Institute for Reference Materials and Measurements, Retieseweg 111, B-2440 Geel, Belgium.
**Present address: National Superconducting Cyclotron Laboratory, Michigan State University, East Lansing, MI 48824-1321, USA.
††Present address: Niigata University, 8050 Ikarashi 2-no-cho, Nishi-ku, 950-2181 Niigata, Japan.

proton-knockout reaction channels. In some cases, we could also measure multinucleon-knockout processes or the production of neutron-rich nuclei by fragmentation.

The general characteristics of the fragmentation reactions have been relatively well known since the 1980s [29]. This reaction mechanism allows us to produce secondary exotic beams over a large range in neutron excess that, together with the use of advanced detection setups, permits us to investigate knockout reactions with high detection efficiency and precision.

The measurements presented in this work are compared with different model calculations that take into account the de-excitation of the knockout remnants. These calculations are used to address several issues, such as the energy dissipated in peripheral fragmentation reactions, the role of nuclear excitations in nucleon knockout, and the evolution of this process with the neutron excess.

II. EXPERIMENT

The experiment was performed at the GSI accelerator facilities in Darmstadt (Germany) using the SIS synchrotron and the fragment separator spectrometer (FRS) [30]. Beams of ^{112}Sn and ^{124}Sn ions with intensities around 10^7 ions/s were accelerated at 1*A* GeV. These beams were then guided to the FRS spectrometer to produce, by fragmentation, other unstable tin isotopes. All the stable and radioactive beams were used to investigate knockout processes and fragmentation with the beam of ^{112}Sn.

A. Detection setup

The FRS is a two-stage achromatic magnetic spectrometer with a dispersive intermediate image plane. Each part of the spectrometer consists of two dipoles with its respective quadrupoles and sextupoles. The function of the quadrupoles is to guarantee the optical quality at the focal planes, while the sextupoles are used for correcting the chromatic aberrations. In the present work, we used the FRS in its achromatic mode. The acceptance of this device is about $\pm 1.5\%$ in longitudinal momentum and approximately ± 15 mrad in polar angle around the central trajectory.

The optical features of the FRS and the high quality of the detection systems guarantee the unambiguous separation and identification of the reaction products, according to their mass and atomic numbers [30]. In order to cover a large range in projectile neutron excess, we combined stable tin projectiles (^{112}Sn and ^{124}Sn) with secondary beams of ^{110}Sn and ^{120}Sn produced in the fragmentation of the stable ones.

Stable tin projectiles impinged on a carbon target with a thickness of 100 mg/cm^2, placed at the entrance of the FRS spectrometer [see Fig. 1]. The two stages of the FRS were used to identify proton- and neutron-knockout reaction products. The unstable tin projectiles were produced by fragmentation in a carbon target with a thickness of 978 mg/cm^2, also located at the entrance of the FRS [see Fig. 1]. These unstable tin projectiles were identified and separated by using the first section of the FRS. Then, a second carbon target with a thickness of 1400 mg/cm^2 was placed at the dispersive

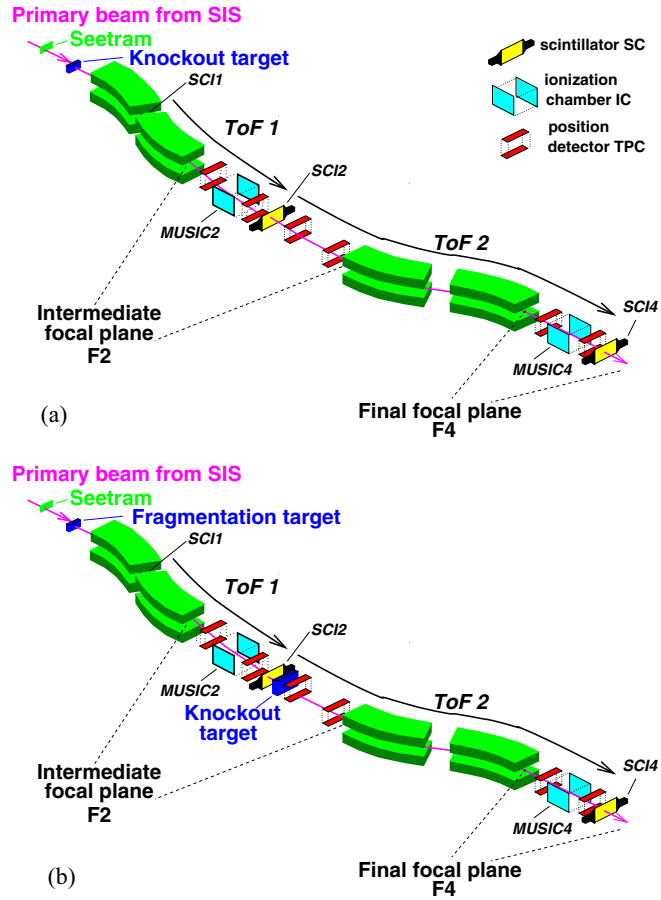

FIG. 1. Schematic view of the FRS experimental setups used in the present work. (a) Setup with the reaction target at the entrance of the spectrometer to investigate knockout reactions of stable tin isotopes (^{112}Sn and ^{124}Sn). (b) Setup with a fragmentation target at the entrance of the FRS to produce secondary beams of ^{110}Sn and ^{120}Sn that then impinged on a second carbon target located at the intermediate focal plane F2 in order to induce knockout reactions.

midplane of the FRS (F2) to induce knockout reactions. Since the intensity of the unstable tin projectiles is lower than the one of the primary beams, we used thicker carbon targets in order to enhance the production. In this latter case, only the second part of the FRS was used to identify the proton- and neutron-removal residues.

In all measurements, the beam intensity was monitored by using the Secondary Electron Transmssion Monitor (SEETRAM) [31] calibrated with a reference plastic scintillator [32]. Three plastic scintillator detectors were placed between the two first dipoles and at the intermediate and final focal planes to measure the time of flight (ToF) of the reaction products with a resolution of around 150 ps full width at half maximum (FWHM). In order to determine the trajectory of each fragment, time projection chambers (TPCs) [33] were placed at the dispersive and final focal planes. The TPCs provide the horizontal (x) and vertical (y) positions in each focal plane with a resolution of 300 μm (FWHM). Finally, the atomic numbers of fragments were determined by measuring

their energy loss in two multiple-sampling ionization chambers (MUSICs) [34] also placed at the dispersive and final focal planes.

B. Identification of the residual nuclei

A complete description of the analysis procedure followed in this work can be found in Refs. [35–37]; here, we just summarize the most important aspects. Nuclei transmitted through the FRS can be identified in mass over atomic number (A/Z) through the determination of their magnetic rigidity $(B\rho)$ and velocity (v) after assuming that they were completely stripped $(q = Z)$, according to the following equation:

$$B\rho = \frac{Au}{qe}\gamma\beta c, \tag{1}$$

where q is the atomic charge state, u is the atomic mass unit, e is the elementary charge, c is the speed of the light, and $\beta = v/c$. In addition, the measurement of the atomic number Z provides the complete identification of the residual nuclei.

The magnetic rigidity $B\rho$ of each reaction product can be obtained in terms of the magnetic-rigidity value of an ion following the central trajectory along the FRS and its position, according to the dispersive coordinate at the intermediate focal plane (F2), using the equation

$$B\rho_2 = B\rho_0^{F2}\left(1 - \frac{x_2}{D_{F2}}\right), \tag{2}$$

where x_2 is the horizontal position at the intermediate focal plane, D_{F2} is the value of the dispersion from the production target until the focal plane F2, and $B\rho_0^{F2}$ is the magnetic rigidity of a central trajectory along the first section of the FRS.

For the final focal plane F4, the magnetic rigidity can be obtained according to

$$B\rho_4 = B\rho_0^{F4}\left(1 - \frac{x_4 - Mx_2}{D_{F4}}\right), \tag{3}$$

where $B\rho_0^{F4}$ is the magnetic rigidity of a central trajectory between F2 and F4, and x_2 and x_4 are the positions at the focal planes F2 and F4, respectively. Finally, D_{F4} is the dispersion between both focal planes F2 and F4, and M is the magnification.

In Eqs. (2) and (3), the magnetic rigidity of the central trajectory, as well as the dispersions and the magnification, were determined by measuring the trajectory of ^{124}Sn projectiles at $1A$ GeV for different values of the magnetic fields in the dipoles of the spectrometer. These measurements allowed us to calibrate the FRS optics, obtaining a dispersion for the middle and final focal planes of $D_{F2} = -7.20$ cm/% and $D_{F4} = 7.40$ cm/%, respectively. These quantities also provided the magnification of the spectrometer according to $M = D_{F4}/D_{F2}$: $M = -1.028$.

Using the above equations, it is possible to determine the mass-over-charge ratio (A/Z) of each transmitted nuclei by combining two independent measurements: their magnetic rigidity $(B\rho)$, determined from the position measurements of the TPC detectors, and their velocity, obtained from the ToF measurements.

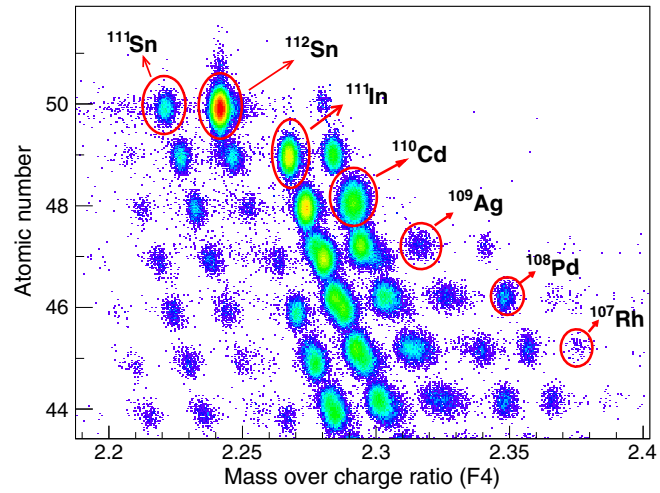

FIG. 2. Identification matrix at the final focal plane (F4) of the FRS obtained in reactions induced by ^{112}Sn impinging on the carbon target. The figure was obtained by overlapping several magnetic settings of the FRS.

Figure 2 displays the identification matrix of the fragmentation residues measured in this experiment by using a beam of ^{112}Sn at $1A$ GeV impinging on a carbon target with a thickness of 978 mg/cm^2. This figure was obtained by overlapping four different magnetic settings of the FRS, centered on ^{112}Sn, ^{112}Cd, ^{111}Cd, and ^{110}Ag. The calibration in atomic and mass number was performed with respect to the signals registered for the beam of ^{112}Sn. The figure shows the good resolution in atomic and mass number achieved in this measurement: $\Delta Z/Z = 7 \times 10^{-3}$ and $\Delta A/A = 2 \times 10^{-3}$ (FWHM), respectively.

In this figure, we identify the production of elements ranging from tin to ruthenium with a clear access to very neutron-rich nuclei. We observe the most neutron-rich nuclei that can be produced in nucleon-removal processes, such as ^{111}In, ^{110}Cd, ^{109}Ag, ^{108}Pd, and ^{107}Rh, corresponding to the removal of up to five protons from ^{112}Sn and no neutron loss. In addition, we also observe the production of ^{112}In that corresponds to (n, p) charge-exchange processes. In this kind of reaction, the quasielastic exchange of protons and neutrons between projectile and target nuclei, or the excitation of nucleon resonances [38,39], increases the number of neutrons in the residual fragment with respect to the initial projectile.

III. RESULTS AND DISCUSSION

Reaction cross sections were obtained by normalizing the production yield of a given residual nucleus to the number of projectiles and target nuclei. The number of incoming projectiles is obtained by using the SEETRAM detector after being calibrated with a reference plastic scintillator. The uncertainty in the determination of the incoming projectiles is around 5%. For unstable ions, the number of projectiles is obtained from the corresponding identification plot at the intermediate focal plane by gating on the fragment of interest. In the latter case, the uncertainty is less than 2%.

The final production yields are obtained from the measured yields corrected by the detection efficiency. This correction can be defined in terms of different factors that are described in the following.

The first correction factor is due to the use of high-intensity beams, which affect the determination of the cross sections because of the acquisition dead time. This correction was evaluated from the ratio between the number of accepted and total triggers registered by the data acquisition system. This value was kept below 30% during the experiment in order to obtain reliable measurements.

Another factor affecting the determination of the production yields is the transmission of a given nucleus through the FRS. As the FRS has a limited momentum acceptance, the complete momentum distributions and consequently the number of total number of residues were not fully transmitted in a specific magnetic setting. This correction factor was obtained by comparison of MOCADI [40] and LISE [41] ion optics calculations and its value was less than 30% with an uncertainty around 10%.

Secondary reactions that occur in different layers of matter along the beam line were also taken into account. The fragments produced in the primary reaction can undergo a second reaction in the target or other layers of matter placed downstream. Because of this, the measured yield of a given residual nucleus will be smaller. In order to calculate this correction factor, it is necessary to determine the total probability of interaction in each layer of matter. A model based on the KAROL code [42] was used to obtain this correction factor. The average value of this correction factor was 1, 6, and 8% for the carbon targets with thicknesses of 100, 987, and 1400 mg/cm^2, respectively.

Finally, a nucleus produced in a reaction can change its atomic charge state due to electromagnetic interactions with the different layers of matter along the beam line. This effect can alter the measurement of the A/q ratio and therefore affects the number of counts used in the determination of the cross section. In order to determine the losses and contaminations due to the atomic charge states of the reaction residues in the first and second stages of the FRS, we used the code GLOBAL [43]. The contribution of the ionic charge state correction in our experiment was less than $\sim$2% with an uncertainty of 1%.

In Table I, we list the one- and two-nucleon removal cross sections, together with their uncertainties, measured for different tin projectiles used in this work. For the stable projectiles (^{112}Sn and ^{124}Sn), we used a carbon target with a thickness of 100 mg/cm^2 (T1), located at the entrance of the FRS. In the case of secondary beams (^{110}Sn and ^{120}Sn), we induced the knockout reactions in a carbon target with a thickness of 1400 mg/cm^2 (T2), placed at the intermediate focal plane of the FRS. The statistical uncertainty of these measurements was below 2%. The total uncertainty was obtained from the quadratic sum of the uncertainties of the different correction factors and the statistical ones, ranging from 7 to 12%.

The experiment also allowed us to determine the cross sections of the most neutron-rich residues produced in cold fragmentation reactions of projectiles of ^{112}Sn at 1A GeV. These cross sections are listed in Table II, together with their corresponding total uncertainties. For these cross sections, the statistical uncertainty ranges from 3 to 48%, depending on the residual nuclei, and the systematic uncertainty fluctuates between 6 and 10%, depending on the transmission.

Figure 3 displays the proton- and neutron-removal cross sections measured in this work (solid circles) together with the measurements performed by Perez-Loureiro *et al.* (open squares) [37] at the FRS, using neutron-rich projectiles of ^{132}Sn at a kinetic energy around 1A GeV impinging on a beryllium target. We also show the data obtained by Audirac *et al.* [22] at RIKEN, using as projectiles ions of ^{104}Sn and ^{112}Sn at kinetic energies of 142A and 161A MeV, respectively, impinging on carbon (open triangles) and hydrogen (solid stars) targets. The good agreement between the cross sections obtained for the nucleon removal from ^{112}Sn in both experiments indicates that the difference in kinetic energy of the projectile may not affect significantly this reaction channel. In addition, we display the measurement performed by Cerizza *et al.* (open cross) [44] for the neutron-removal cross section of ^{107}Sn impinging on a beryllium target at 140A MeV, which is also in good agreement with the tendency of the other data.

In the upper panel, we can see that the neutron-removal cross section increases with the mass number of the projectile, while in the lower panel the proton-removal cross section decreases. We also observe that the increase (decrease) of the neutron (proton)-removal cross sections is faster in the mass-number range from 104 to 110. Qualitatively, the behavior

TABLE I. One- and two-nucleon-removal cross sections for the reactions investigated in this work. These measurements were performed by using two carbon targets with thicknesses of 100 mg/cm^2 (T1) and 1400 mg/cm^2 (T2).

Projectile (target)	Nucleus	σ [mb]	Nucleus	σ [mb]
^{124}Sn (T1)	^{123}Sn	148 $\pm$ 11	^{123}In	20.79 $\pm$ 1.26
^{120}Sn (T2)	^{119}Sn	146 $\pm$ 18	^{119}In	23.56 $\pm$ 2.90
	^{118}Cd	1.10 $\pm$ 0.14		
^{112}Sn (T1)	^{111}Sn	139 $\pm$ 10	^{111}In	40.2 $\pm$ 2.8
^{110}Sn (T2)	^{109}Sn	135 $\pm$ 16	^{109}In	47.1 $\pm$ 5.6
	^{108}Cd	9.9 $\pm$ 1.2		

TABLE II. Cross sections of the most neutron-rich residues measured in this work for the fragmentation of ^{112}Sn. The reactions were produced in a carbon target with a thickness of 978 mg/cm^2.

Nucleus	σ [mb]	Nucleus	σ [mb]
^{111}Cd	0.699 $\pm$ 0.084	^{107}Pd	0.113 $\pm$ 0.019
^{110}Cd	3.11 $\pm$ 0.35	^{106}Pd	0.596 $\pm$ 0.080
^{109}Cd	7.46 $\pm$ 0.82	^{105}Pd	1.25 $\pm$ 0.11
^{110}Ag	0.031 $\pm$ 0.009	^{107}Rh	0.0004 $\pm$ 0.0002
^{109}Ag	0.157 $\pm$ 0.021	^{106}Rh	0.016 $\pm$ 0.003
^{108}Ag	1.08 $\pm$ 0.12	^{105}Rh	0.08 $\pm$ 0.01
^{107}Ag	3.04 $\pm$ 0.31	^{104}Rh	0.319 $\pm$ 0.055
^{108}Pd	0.0089 $\pm$ 0.0021	^{103}Rh	1.10 $\pm$ 0.11

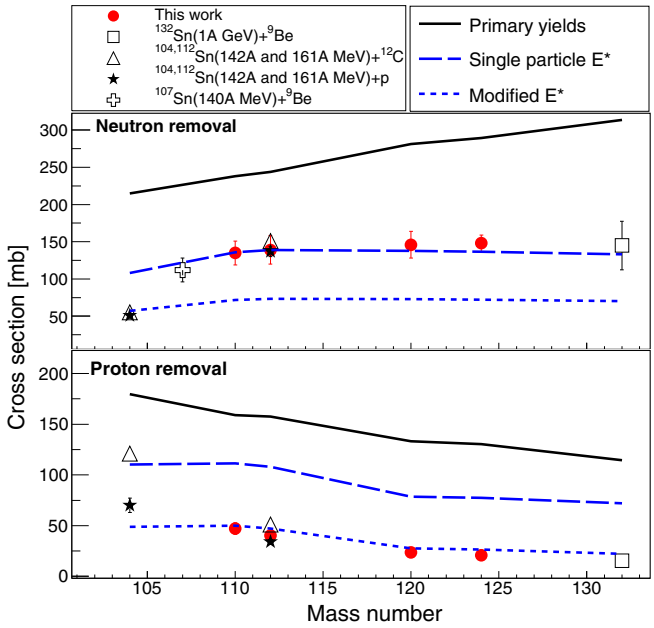

FIG. 3. Neutron-removal (upper panel) and proton-removal (lower panel) cross sections measured for different tin isotopes covering a large range in neutron excess: Perez-Loureiro *et al.* (open squares) [37], Audirac *et al.* (open triangles and solid stars) [22], Cerizza *et al.* (open cross) [44], and this work (solid dots). The data uncertainties are shown if they exceed the size of the symbols. This set of data is compared with Glauber model calculations (lines).

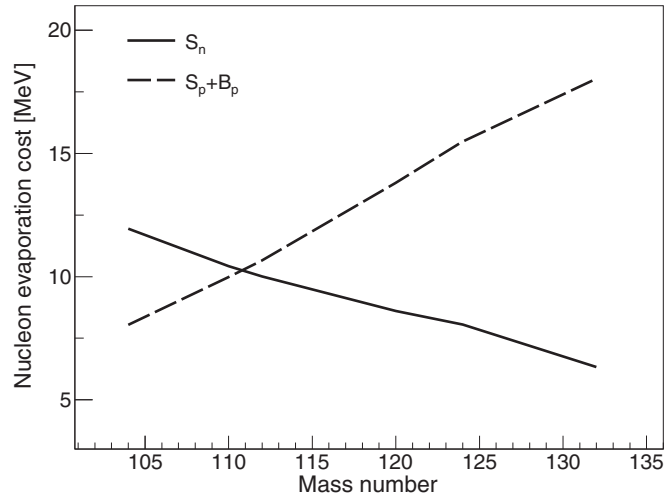

FIG. 4. Energy cost for the emission of neutrons (binding energy, solid line) and protons (binding and Coulomb energy, dashed line) of the remnants produced in the proton-knockout reactions studied in this work as a function of the tin projectile mass number. Similar results are obtained for the neutron-knockout remnants.

of these cross sections could be explained by the number of neutrons and protons at the surface of the projectile and by the proton and neutron binding energies. On one hand, because we deal with an isotopic chain, the number of protons at the surface of the nucleus can be assumed constant, while the number of neutrons increases moving from ^{104}Sn to ^{132}Sn. On the other hand, the neutron (proton) binding energy decreases (increases) when we increase the mass number of the projectile (see Fig. 4). These two facts enhance the one neutron-removal probability when we move from ^{104}Sn to ^{132}Sn and could also explain the decrease observed for the one proton-removal cross sections.

For isotopes close to ^{100}Sn, one could expect similar values for the proton- and neutron-removal cross sections, as it is observed for ^{104}Sn impinging on a hydrogen target. However, the proton-removal cross section with a carbon target is 43% larger than the neutron-removal one. In addition, the neutron-removal cross sections for ^{104,112}Sn and the proton-removal cross section for ^{112}Sn present a dependence with the target below 9%. This discrepancy could be explained by the electromagnetic interaction between the projectile and target nuclei, leading to remnants with an excitation energy of around 11 MeV [45] that should have a larger probability with the carbon target. Because the proton binding energy for ^{104}Sn is lower than the neutron one [46], the emission of one proton becomes more likely, increasing the proton removal cross section with respect to the neutron one.

For a better understanding of the neutron- and proton-removal cross sections, we overlay the data of Fig. 3 with different model calculations. Fragmentation reactions at relativistic energies are often described by means of a two-step process [47]: the collision itself, where part of the mass is removed from projectile and target nuclei and excitation energy is gained by the surviving remnants, and subsequent de-excitation processes by the evaporation of γ rays, nucleons, and light nuclei.

In this work, we use an abrasion model to describe single- and multiple-knockout processes in nucleus-nucleus collisions, similar to that described in previous works, such as in Ref. [48] or in Sec. 8.3 of Ref. [49]. Assuming that at relativistic energies the bombarding energy is well above the Fermi energy, the collision can be described in terms of Glauber's picture [50]. Under this assumption, only the nucleons in the overlap region between the projectile and the target nuclei (participants) interact strongly, while the nucleons outside this zone (spectators) remain undisturbed.

The idea behind the abrasion model is very simple: Whenever a binary collision occurs, the participant nucleons are ejected from the projectile (Z_P, N_P). This assumption allows one to calculate the cross sections for the production of primary fragments with proton and neutron numbers (Z_f, N_f) by means of the simple probabilistic description:

$$\sigma_{\text{abrasion}} = \mathcal{N}(Z_P, N_P; Z_f, N_f) \int d^2b [1 - P_p(\mathbf{b})]^{Z_P - Z_f} \times P_p(\mathbf{b})^{Z_f} [1 - P_n(\mathbf{b})]^{N_P - N_f} P_n(\mathbf{b})^{N_f}. \quad (4)$$

In this equation, Z_f protons from the projectile survive the collision, while $Z_p - Z_f$ protons are removed and the total probability includes the product with an analogous probability for the surviving neutrons N_f in the fragment. The factor $\mathcal{N}(Z_P, N_P; Z_f, N_f) = \binom{Z_P}{Z_f}\binom{N_P}{N_f}$, with $\binom{N}{n}$ equal to the binomial coefficient, accounts for all possible combinations to obtain Z_f protons out of the original Z_p protons, and similarly for the

neutrons. This abrasion cross section is used later as an input for the ablation stage.

The probabilities for single-nucleon survival are given by P_p for protons and P_n for neutrons, with the probability that a proton does not collide with the target given by

$$P_p(\mathbf{b}) = \int ds dz \rho_p^P(\mathbf{s},z) \exp\left[-\sigma_{pp} Z_T \int dz \rho_p^T(\mathbf{b}-\mathbf{s},z) - \sigma_{pn} N_T \int dz \rho_n^T(\mathbf{b}-\mathbf{s},z)\right]. \quad (5)$$

In this equation, σ_{pp} and σ_{np} are the proton-proton (Coulomb removed) and proton-neutron total cross sections, obtained from a fit of experimental data in the energy range of $E_{lab} = 10$–5000 MeV as in Eqs. (1) and (2) of Ref. [51]. $\rho_p^{(P,T)}$ ($\rho_n^{(P,T)}$) are the proton (neutron) densities in the projectile and in the target, respectively. They are normalized so that $\int d^3r \rho_{p(n)}^{P(T)}(\mathbf{r}) = 1$. These densities are generated by the Hartree-Fock Bogoliubov procedure [52,53]. One can use the projectile ground-state densities in the calculation since the mean-field rearrangements that would modify them do not have time to occur until long after the abrasion stage has passed. A similar expression as in Eq. (5) holds for neutron survival.

This procedure has been also used in one-nucleon knockout reactions with success [54], but we have constructed a separate code to perform the calculations in Eqs. (4) and (5). It is also important to notice that here we neglect effects of nucleon-nucleon correlations, such as short-range correlations, which may become important for multinucleon knockout. The excitation energy of the fragments is calculated from the particle-hole energies of the configuration relative to the ground state of each fragment. The energies are calculated with a harmonic oscillator model with $\hbar\omega = 40/\mathrm{A}^{1/3}$ MeV. Each hole corresponds to a vacant state during the abrasion process and the density of states $\rho(E_x, Z_f, A_f)$ is obtained by counting all combinations of holes consistent with the fragment charge and mass numbers. The excitation cross sections for a given excitation energy E_x are given by $d\sigma/dE_x = \rho(E_x, Z_f, A_f)\sigma_{\mathrm{abrasion}}$. These excitation cross sections are used in the de-excitation stage following the abrasion where the decay probabilities are calculated for each excitation energy E_x of the fragment. The density of states $\rho(E_x, Z_f, A_f)$ naturally includes the factor $\mathcal{N}(Z_P, N_P; Z_f, N_f)$ defined previously. Therefore, in the calculation of $d\sigma/dE_x$, the latter factor is omitted when calculating Eq. (4).

Unbound remnants are de-excited using the ABLA07 code [55], which describes the de-excitation of a nucleus emitting γ rays, neutrons, light-charged particles, and intermediate-mass fragments (IMFs) according to Weisskopf's formalism [28]. For a more realistic description of the de-excitation, the separation energies and the emission barriers for charged particles are also considered according to the atomic mass evaluation from 2016 [56] and the Bass potential [57], respectively. In addition, de-excitation by fission is also included according to a dynamical picture described in Refs. [58,59]. These model calculations have been bench marked in several works by using isotopic distributions of evaporation residues and fission fragments produced in spallation and fragmentation reactions of nuclei from iron to uranium, providing a satisfactory description of many observables [60–69].

In Fig. 3, we try to describe the new data with these model calculations. For this purpose, we compare the neutron (upper panel) and proton (lower panel) knockout cross sections with the Glauber model coupled to the evaporation code ABLA07. The solid line represents the results of calculations neglecting core excitations in the knockout process (primary yields). Then, we performed calculations where the excitation energy of the remnants is obtained from the single-particle–hole picture (dashed lines). Finally, we also performed calculations increasing arbitrarily the excitation energy of the remnants produced in proton and neutron knockout by 7 and 4 MeV, respectively (dotted lines).

As can be seen in the figure, the neutron knockout is nicely described when considering standard particle-hole excitations, except for the most neutron-deficient nuclei. Conversely, the same calculations overpredict the proton-knockout process, except for the most neutron-deficient nuclei. One can explain the tendencies as a competition between the probability of the primary yields and the survival probability of the remnants in the de-excitation stage that is strongly governed by the minimum in the energy cost for proton (binding and Coulomb energy, dashed line) and neutron (binding energy, solid line) emission. In Fig. 4, we display this energy cost for the remnants produced in the proton- and neutron-knockout reactions as a function of the projectile mass number. We can see that the low neutron-separation energies of the remnants between ^{112}Sn and ^{132}Sn compensate for the large cross sections of the primary yields, resulting in similar neutron-knockout cross sections for all those isotopes (see Fig. 3). For projectiles between ^{104}Sn and ^{110}Sn, the neutron-knockout cross sections decrease with the mass of the projectile because of the reduction in the primary yields but also in the proton emission energy cost. For the proton knockout, both the cross sections of the primary yields and the nucleon emission energy cost only contribute to decreasing the cross sections with the mass number of the projectile. Therefore, we observe a constant decrease of the final cross section with the mass number.

We then conclude that calculations considering standard particle-hole excitations overpredict the measured cross sections for the knockout of deeply bound nucleons. Similar results obtained in electron- [2] and nucleon-induced [14] knockout reactions were explained in terms of correlations. Indeed, around 50% overprediction of the cross section that we observe in the proton knockout with stable and neutron-rich tin isotopes is in reasonable agreement with the observed reduction in the corresponding spectroscopic factors in $(e,e'p)$ reactions with stable nuclei. Regardless of the process responsible for the observed deviations with respect to the standard particle-hole excitations, the measured cross sections can be explained increasing the excitation energies induced by the proton and neutron knockout in neutron-rich and neutron-deficient nuclei, respectively.

This finding is also in agreement with the conclusions found in previous works where abrasion-evaporation model calculations were used to investigate multiproton-knockout cross sections of neutron-rich nuclei, such as ^{132}Sn [37], ^{136}Xe [36], ^{197}Au [70,71], ^{208}Pb [72], and ^{238}U [73]. In those works,

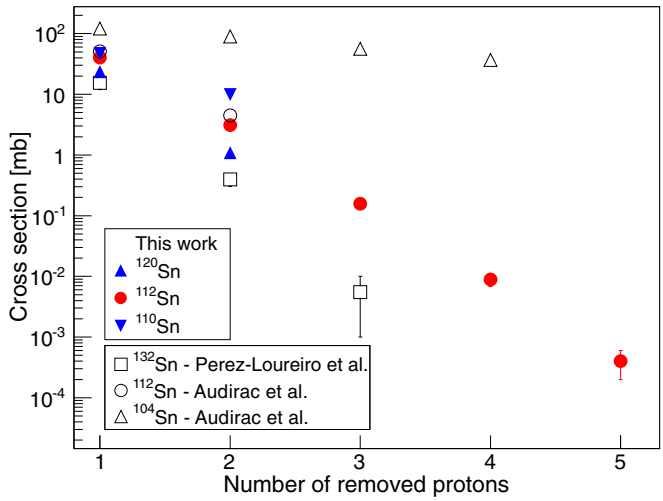

FIG. 5. Cross sections of the proton-removal channels produced in the fragmentation of different tin isotopes measured by Perez-Loureiro *et al.* (open squares) [37], Audirac *et al.* (open circles and triangles) [22], and this work (solid symbols). The data uncertainties are shown if they exceed the size of the symbols.

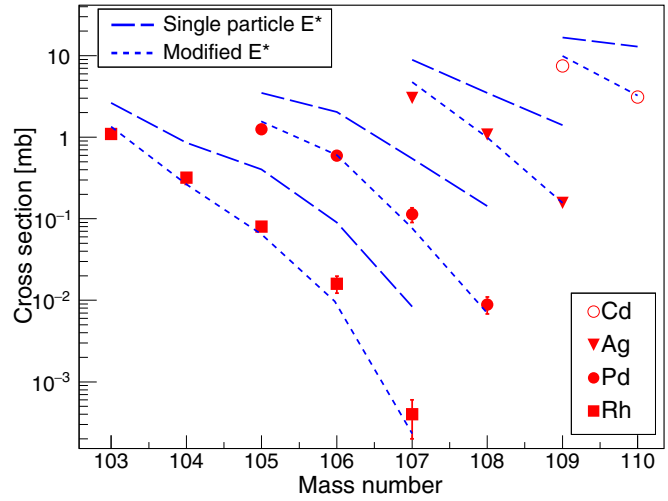

FIG. 6. Measured isotopic production cross sections of fragment residues produced in the reaction ^{112}Sn (1A GeV) + ^{12}C (points) compared with different calculations (lines). The data uncertainties are shown if they exceed the size of the symbols.

an increase of the particle-hole excitation energy was also required to describe the isotopic distributions of fragmentation residues close in mass number to the projectile [72–74].

Following these ideas, in Fig. 5 we display the multiproton-removal cross section as a function of the number of removed protons for different tin isotopes from ^{104}Sn to ^{132}Sn. We can see that the cross sections decrease systematically with the number of removed nucleons from a given nucleus, but also with its mass number as observed for the proton-knockout cross sections (see lower panel of Fig. 3). These measurements confirm that the probability for removing protons is larger when the neutron-to-proton ratio equilibrates at the surface of the nucleus. Complementary results were obtained by Audirac *et al.* [22] for multineutron-knockout cross sections induced in tin isotopes. They found that the multineutron-removal cross sections increase with the mass number of the projectile, as we observe for the one-neutron-removal cross sections displayed in the upper panel of Fig. 3.

Finally, in Fig. 6 we depict the production cross sections of the most neutron-rich residues produced by the removal of nucleons in fragmentation reactions of ^{112}Sn projectiles at 1A GeV impinging on a carbon target. In the figure, we also display similar calculations to the ones presented in Fig. 3. These calculations show that the most neutron-rich residues produced in multiproton-removal reactions can only be described by increasing the average excitation energy obtained from particle-hole excitations (dotted lines), as concluded from Fig. 3. Nuclei with a more balanced number of proton and neutrons can be described by particle-hole excitations (dashed lines).

The comparison of the cross sections presented in this work with Glauber model calculations, covering a large range in neutron excess and excitation energy, clearly indicates that nuclear excitations play an important role in the removal of deeply bound nucleons, as pointed out in other works [22–25,70,74]. It seems also clear that the removal of deeply bound nucleons enhances the excitation energy gained by the remnants. These higher values of excitation energy could be an indication of the role of nucleon-nucleon correlations [2,14].

IV. SUMMARY AND CONCLUSIONS

The residual nuclei produced in nucleon-knockout and fragmentation reactions induced by projectiles of tin isotopes covering a large range in neutron excess were investigated in inverse kinematics using the FRS at GSI. The high resolution of this spectrometer combined with a highly efficient detection system allowed us to unambiguously identify the reaction products. These data were completed with previous measurements at GSI, using ^{132}Sn projectiles, and at RIKEN, using ^{110}Sn and ^{112}Sn. The good agreement between the one-nucleon removal cross sections for ^{112}Sn measured at RIKEN and GSI would indicate that the different projectile energies do not seem to affect the reaction mechanism, at least above 140A MeV.

The dependence of the measured proton- and neutron-knockout cross sections with the mass number of the tin projectiles can be explained considering the evolution of the abundances of proton and neutrons at the nuclear periphery, and the proton and neutron binding energies of the primary knockout remnants. According to this interpretation, remnant excitations are relevant for the understanding of the final cross sections.

The comparison of the measurements with Glauber model calculations shows a clear overprediction of the cross sections for the knockout of deeply bound nucleons (protons in neutron-rich systems and neutrons in neutron-deficient ones). The observed overprediction is similar to the one obtained in electron-induced proton knockout with stable nuclei and explained as due to nuclear correlations, affecting the single-particle spectroscopic strengths, which are not considered in the model calculations. We also confirm that this overprediction only affects the knockout of deeply bound nucleons. Finally, we describe those effects by a phenomenological increase of the excitation energy induced in the knockout of

deeply bound nucleons. This conclusion also applies for the description of fragmentation residual nuclei.

ACKNOWLEDGMENTS

The authors are grateful to the GSI accelerator staff for providing intense and stable beams of ^{112}Sn and ^{124}Sn. This work was partially supported by the Spanish Ministry of Economy and Competitiveness under Projects No. FPA2013-47831-C2-1-P, No. FPA2015-69640-C2-1-P, and Consolider-CPAN-CSD2007-00042, and by the Regional Government of Galicia under the program "Grupos de Referencia Competitiva 2013-011". C.A.B. acknowledges support from US NSF Grant No. 1415656 and US DOE Grant No. DE-FG02-08ER41533.

[1] G. Jacob and Th. A. J. Maris, Rev. Mod. Phys. **38**, 121 (1966).
[2] V. R. Pandharipande, I. Sick, and P. K. A. deWitt Huberts, Rev. Mod. Phys. **69**, 981 (1997).
[3] T. Kobayashi, O. Yamakawa, K. Omata, K. Sugimoto, T. Shimoda, N. Takahashi, and I. Tanihata, Phys. Rev. Lett. **60**, 2599 (1988).
[4] R. Anne *et al.*, Phys. Lett. B **304**, 55 (1993).
[5] J. H. Kelley *et al.*, Phys. Rev. Lett. **74**, 30 (1995).
[6] T. Aumann, C. A. Bertulani, and J. Ryckebusch, Phys. Rev. C **88**, 064610 (2013).
[7] M. B. Tsang, J. Lee, and W. G. Lynch, Phys. Rev. Lett. **95**, 222501 (2005).
[8] I. Tanihata, H. Hamagaki, O. Hashimoto, Y. Shida, N. Yoshikawa, K. Sugimoto, O. Yamakawa, T. Kobayashi, and N. Takahashi, Phys. Rev. Lett. **55**, 2676 (1985).
[9] P. G. Hansen and J. A. Tostevin, Annu. Rev. Nucl. Part. Sci. **53**, 219 (2003).
[10] I. Tahihata, Nucl. Phys. A **685**, 80 (2001).
[11] A. Navin *et al.*, Phys. Rev. Lett. **81**, 5089 (1998).
[12] T. Aumann *et al.*, Phys. Rev. Lett. **84**, 35 (2000).
[13] D. Cortina-Gil *et al.*, Phys. Lett. B **529**, 36 (2002).
[14] A. Gade *et al.*, Phys. Rev. Lett. **93**, 042501 (2004).
[15] R. Kanungo *et al.*, Phys. Rev. Lett. **102**, 152501 (2009).
[16] F. Flavigny, A. Obertelli, A. Bonaccorso, G. F. Grinyer, C. Louchart, L. Nalpas, and A. Signoracci, Phys. Rev. Lett. **108**, 252501 (2012).
[17] N. Kobayashi *et al.*, Phys. Rev. C **93**, 014613 (2016).
[18] C. A. Bertulani and P. G. Hansen, Phys. Rev. C **70**, 034609 (2004).
[19] A. Gade *et al.*, Phys. Rev. C **77**, 044306 (2008).
[20] J. Lee *et al.*, Phys. Rev. Lett. **104**, 112701 (2010).
[21] F. Flavigny *et al.*, Phys. Rev. Lett. **110**, 122503 (2013).
[22] L. Audirac *et al.*, Phys. Rev. C **88**, 041602(R) (2013).
[23] C. Louchart, A. Obertelli, A. Boudard, and F. Flavigny, Phys. Rev. C **83**, 011601(R) (2011).
[24] Y. L. Sun *et al.*, Phys. Rev. C **93**, 044607 (2016).
[25] A. Deltuva, A. Ross, E. Norvaišas, and F. M. Nunes, Phys. Rev. C **94**, 044613 (2016).
[26] R. Thies *et al.*, Phys. Rev. C **93**, 054601 (2016).
[27] J. J. Gaimard and K.-H. Schmidt, Nucl. Phys. A **531**, 709 (1991).
[28] V. F. Weisskopf and D. H. Ewing, Phys. Rev. **57**, 472 (1940).
[29] J. Hüfner, Phys. Rep. **125**, 129 (1985).
[30] H. Heissel *et al.*, Nucl. Instr. Methods Phys. Res., Sect. B **70**, 286 (1992).
[31] A. Junghans *et al.*, Nucl. Instr. Methods Phys. Res., Sect. A **370**, 312 (1996).
[32] B. Voss *et al.*, Nucl. Instr. Methods Phys. Res., Sect. A **364**, 150 (1995).
[33] R. Janik *et al.*, Nucl. Instrum. Methods Phys. Res., Sect. A **640**, 54 (2011).
[34] M. Pfüzner *et al.*, Nucl. Instrum. Methods Phys. Res., Sect. B **86**, 213 (1994).
[35] E. Casarejos *et al.*, Phys. Rev. C **74**, 044612 (2006).
[36] J. Benlliure *et al.*, Phys. Rev. C **78**, 054605 (2008).
[37] D. Perez-Loureiro *et al.*, Phys. Lett. B **703**, 552 (2011).
[38] J. Chiba *et al.*, Phys. Rev. Lett. **67**, 1982 (1991).
[39] A. I. Morales *et al.*, Phys. Rev. C **88**, 014319 (2013).
[40] C. Scheidenberger *et al.*, Phys. Rev. Lett. **77**, 3987 (1996).
[41] D. Bazin *et al.*, Nucl. Instrum. Methods Phys. Res., Sect. A **482**, 307 (2002).
[42] P. J. Karol, Phys. Rev. C **11**, 1203 (1975).
[43] C. Scheidenberger *et al.*, Nucl. Instrum. Methods Phys. Res., Sect. B **142**, 441 (1998).
[44] G. Cerizza *et al.*, Phys. Rev. C **93**, 021601(R) (2016).
[45] G. Baur and C. A. Bertulani, Phys. Rev. C **34**, 1654 (1986).
[46] G. Audi, M. Wang, A. H. Wapstra, F. G. Kondev, M. MacCormick, X. Xu, and B. Pfeiffer, Chin. Phys. C **36**, 1287 (2012).
[47] R. Serber, Phys. Rev. **72**, 1114 (1947).
[48] J. Hüfner, K. Schäfer, and B. Schüman, Phys. Rev. C **12**, 1888 (1975).
[49] C. A. Bertulani and P. Danielewicz, *Introduction to Nuclear Reactions* (IOP, London, 2004).
[50] R. J. Glauber and G. Matthiae, Nucl. Phys. B **21**, 135 (1970).
[51] C. A. Bertulani and C. De Conti, Phys. Rev. C **81**, 064603 (2010).
[52] P. Avogadro and T. Nakatsukasa, Phys. Rev. C **84**, 014314 (2011).
[53] P. Avogadro and C. A. Bertulani, Phys. Rev. C **88**, 044319 (2013).
[54] C. A. Bertulani and A. Gade, Comp. Phys. Comm. **175**, 372 (2006).
[55] A. Kelić, M. V. Ricciardi, and K.-H. Schmidt, in *Proceedings of Joint ICTP-IAEA Advanced Workshop on Model Codes for Spallation Reactions, ICTP Trieste, Italy, 4-8 February 2008*, edited by D. Filges, S. Leray, Y. Yariv, A. Mengoni, A. Stanculescu, and G. Mank (IAEA, Vienna, 2008), pp. 181–221.
[56] W. J. Huang, G. Audi, M. Wang, F. G. Kondev, S. Naimi, and X. Xu, Chin. Phys. C **41**, 030002 (2017).
[57] R. Bass, *Proceedings of the Symposium on Deep-Inelastic and Fusion Reactions with Heavy Ions* (Springer-Verlag, Berlin, 1980).
[58] B. Jurado, K.-H. Schmidt, and J. Benlliure, Phys. Lett. B **553**, 186 (2003).
[59] B. Jurado, C. Schmitt, K.-H. Schmidt, J. Benlliure, and A. R. Junghans, Nucl. Phys. A **747**, 14 (2005).
[60] M. V. Ricciardi *et al.*, Phys. Rev. C **73**, 014607 (2006).

[61] C. Villagrasa-Canton *et al.*, Phys. Rev. C **75**, 044603 (2007).
[62] D. Mancusi, A. Boudard, J. Cugnon, J.-C. David, T. Gorbinet, and S. Leray, Phys. Rev. C **84**, 064615 (2011).
[63] J. Alcántara-Núñez *et al.*, Phys. Rev. C **92**, 024607 (2015).
[64] B. Jurado, C. Schmitt, K.-H. Schmidt, J. Benlliure, T. Enqvist, A. R. Junghans, A. Kelić, and F. Rejmund, Phys. Rev. Lett. **93**, 072501 (2004).
[65] J. Benlliure, E. Casarejos, J. Pereira, and K.-H. Schmidt, Phys. Rev. C **74**, 014609 (2006).
[66] C. Schmitt, K.-H. Schmidt, A. Kelić, A. Heinz, B. Jurado, and P. N. Nadtochy, Phys. Rev. C **81**, 064602 (2010).
[67] Y. Ayyad *et al.*, Phys. Rev. C **89**, 054610 (2014).
[68] Y. Ayyad *et al.*, Phys. Rev. C **91**, 034601 (2015).
[69] J. L. Rodríguez-Sánchez *et al.*, Phys. Rev. C **91**, 064616 (2015).
[70] J. Benlliure *et al.*, Nucl. Phys. A **660**, 87 (1999).
[71] K.-H. Schmidt *et al.*, Nucl. Phys. A **542**, 699 (1992).
[72] T. Kurtukian-Nieto *et al.*, Phys. Rev. C **89**, 024616 (2014).
[73] M. de Jong *et al.*, Nucl. Phys. A **628**, 479 (1998).
[74] K.-H. Schmidt *et al.*, Phys. Lett. B **300**, 313 (1993).